BIOSYNTHESIS

Modular polyketide synthase contains two reaction chambers that operate asynchronously

Saket R. Bagde^{1,2}, Irimpan I. Mathews³, J. Christopher Fromme^{2*}, Chu-Young Kim^{1,4*}

Type I modular polyketide synthases are homodimeric multidomain assembly line enzymes that synthesize a variety of polyketide natural products by performing polyketide chain extension and β -keto group modification reactions. We determined the 2.4-angstrom-resolution x-ray crystal structure and the 3.1-angstrom-resolution cryo–electron microscopy structure of the Lsd14 polyketide synthase, stalled at the transacylation and condensation steps, respectively. These structures revealed how the constituent domains are positioned relative to each other, how they rearrange depending on the step in the reaction cycle, and the specific interactions formed between the domains. Like the evolutionarily related mammalian fatty acid synthase, Lsd14 contains two reaction chambers, but only one chamber in Lsd14 has the full complement of catalytic domains, indicating that only one chamber produces the polyketide product at any given time.

olyketide natural products are bioactive molecules that are widely used and effective in medicine. This class of molecules includes erythromycin (an antibiotic), rapamycin (an immunosuppressant), and epothilone (a chemotherapeutic). Polyethers, a subgroup of polyketide natural products, are characterized by the presence of multiple cyclic ether groups in their structure. Natural polyethers vary in the number, size, and arrangement of the cyclic ether groups they contain. However, all polyethers are thought to be generated in nature through a common threestage biosynthetic scheme (1): Stage 1 is the construction of the polyketide backbone by modular polyketide synthases (PKSs), stage 2 is the stereoselective epoxidation of the polyene intermediate by a monooxygenase, and stage 3 is the formation of the hallmark cyclic ether groups by one or more epoxide hydrolases.

Modular PKSs synthesize polyketides by performing successive Claisen-like condensation reactions (2,3). They are responsible for the biosynthesis of polyether polyketide, nonpolyether polyketide, and polyketide-nonribosomal peptide hybrid natural products. PKS modules minimally contain three functional domains, ketosynthase (KS), acyltransferase (AT), and acyl carrier protein (ACP), which together perform polyketide chain extension. One or more noncondensing domains, namely ketoreductase (KR), dehydratase (DH), and enoylreductase (ER), can transform the β -keto group formed during the condensation step to a hydroxyl, alkene, and methylene, respectively. Multi-

ple modules act successively in an assembly-line-like fashion in which each module performs a single round of chain extension, followed by β -keto group modification reaction, and then transfers the growing polyketide chain to the next module. The final PKS module in the biosynthesis pathway typically contains a thioesterase (TE) domain that catalyzes release of the fully extended polyketide product.

Modular PKSs are structurally and functionally homologous to the mammalian and metazoan fatty acid synthase (4-7). However, fatty acid synthase performs iterative rounds of chain extension and produces a fully reduced alkyl chain, whereas each module of modular PKS performs a single-chain extension cycle and generates a reduced product. Additionally, only modular PKSs contain an N-terminal docking domain (DD) that facilitates inter-PKS communication. In both modular PKSs and mammalian fatty acid synthases, the growing alkyl chain remains attached to the enzyme until it is fully extended and processed. The growing chain is covalently attached to the phosphopantetheine (P-pant) group of the ACP domain. During the reaction cycle, ACP constantly changes its position, which enables all catalytic domains present in these mega enzymes to act on the growing chain. Therefore, the movement of ACP and the specific interactions that ACP forms with other domains is critical for polyketide and fatty acid production. Previous crystallographic studies of modular PKSs were conducted on proteolytic fragments and recombinantly expressed individual domains. Although these investigations have vielded important information on each domain, the three-dimensional organization of multiple domains and the nature of domain-domain interactions in an intact modular PKS are poorly defined. To address this knowledge gap, we selected the lasalocid A antibiotic biosynthesis pathway from Streptomyces lasalocidi as a model system for studying polyether biogenesis (fig. S1A). This pathway consists of seven modular PKSs (Lsd11 to Lsd17) that act sequentially to construct the dodecaketide backbone of lasalocid A from five malonyl-CoA, four methylmalonyl-CoA, and three ethylmalonyl-CoA units (8). Additionally, a flavin-dependent monooxygenase, Lsd18, converts the two *E*-olefins in the polyketide backbone into epoxides (9), and an epoxide hydrolase, Lsd19, transforms the epoxides into cyclic ether groups (10). We have previously reported the characterization of Lsd19 (11, 12), and here we present the structural study of the Lsd14 modular PKS.

We first determined the crystal structure of apo-Lsd14 at 2.4-Å resolution, which revealed that Lsd14's eight catalytic domains form two unequal reaction chambers. This was an unexpected finding because all previous modular PKS models depict a symmetric architecture. In our crystal structure, ACP is docked to the AT, which is expected to occur during the transacylation step (fig. S1B). Because we could only crystallize Lsd14 in this conformation, we turned to cryo-electron microscopy (cryo-EM) to study alternative conformations of Lsd14. This effort yielded the 3.1-Å-resolution cryo-EM structure of holo-Lsd14 in which ACP is docked to the KS, which is expected to occur during the condensation step (fig. S1B). The Lsd14 crvo-EM structure also has an asymmetric architecture, further validating that the two reaction chambers adopt different conformations. Our work highlights the complementary nature of protein x-ray crystallography and cryo-EM techniques.

X-ray crystal structure of apo-Lsd14 stalled at the transacylation step

We solved the x-ray crystal structure of apo-Lsd14 at 2.4-Å resolution (Fig. 1, fig. S2, and table S1, PDB 7S6B). Lsd14 is a single-module PKS composed of a pair of KS, AT, KR, and ACP domains. Seven of the eight functional domains that constitute the Lsd14 homodimer are clearly visible in the electron density map and could be modeled. One ACP domain was not detected, presumably because it is not locked into a single position. Additionally, parts of the AT-to-KR and KR-to-ACP linker were not visible in the electron density map (table S2), so the polypeptide chain identity of KR and ACP remained unassigned. We labeled the equivalent domains in Lsd14 with and without the prime symbol (') for clarity. However, only DD-KS-LD-AT-PAL (chain A) and DD'-KS'-LD'-AT'-PAL' (chain B) have been crystallographically confirmed to reside on the same polypeptide chain.

Lsd14 has a compact homodimeric structure, with the dimer interface formed by DD/DD' (~524 Ų), KS/KS' (~1952 Ų), and pre-KR dimerization element (DE), DE/DE' (~826 Ų) (Fig. 1). The post-ACP dimerization element (ADE), which is not visible in the current structure, may provide

Department of Chemistry and Biochemistry, The University of Texas at El Paso, El Paso, TX 79968, USA. Department of Molecular Biology and Genetics/Weill Institute for Cell and Molecular Biology, Cornell University, Ithaca, NY 14853, USA. Stanford Synchrotron Radiation Lightsource, SLAC National Accelerator Laboratory, Stanford University, Menlo Park, CA 94025, USA. Border Biomedical Research Center, The University of Texas at El Paso, El Paso, TX 79968, USA. Corresponding author. Email: ckim7@utep.edu (C.-Y.K.); icf14@cornell.edu (J.C.F.)

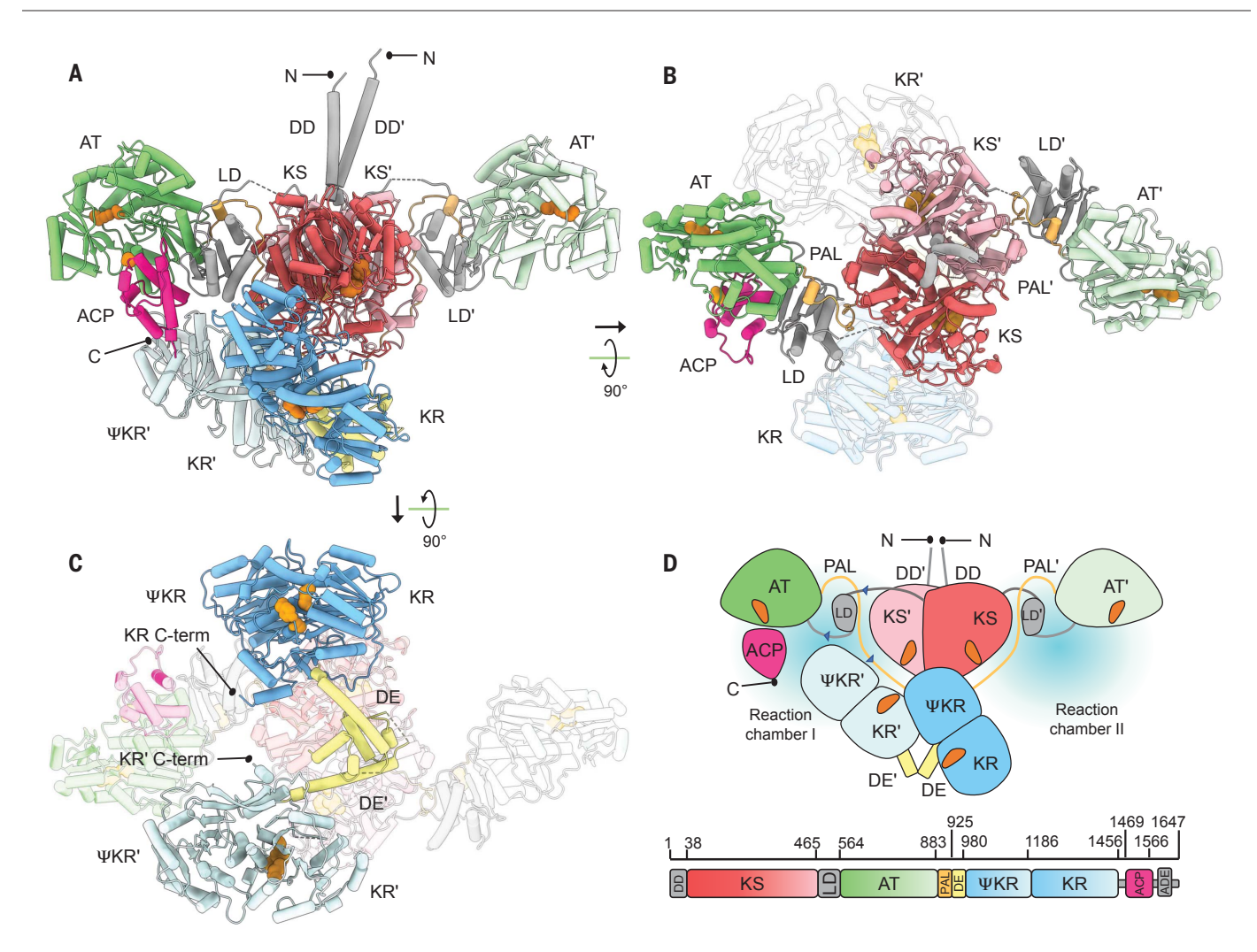


Fig. 1. Crystal structure of Lsd14. (**A** to **C**) Side view (A), top view (B), and bottom view (C) of Lsd14. Active site residues of each domain are shown in orange. (**D**) Cartoon representation and linear organization of Lsd14. ΨKR, KR structural subdomain.

additional contact surface area. The two AT domains lie on opposite ends of the KS dimer and are connected to the KS by a highly ordered linker domain (LD). The post-AT linker (PAL) loops back to the KS before connecting with the KR (fig. S3, A to E). The KS-LD-AT/KS'-LD'-AT' dimer, hereby designated as (KS-LD-AT)2, forms an extended structure with a twofold symmetry that mirrors the previously reported crystal structures of the (KS-LD-AT)₂ fragments from 6-deoxyerythronolide B synthase (DEBS) module 3 (PDB 2QO3), DEBS module 5 (PDB 2HG4), and curacin synthase module CurL (PDB 4MZ0) (fig. S3F) (13-15). The two KR domains are located below the (KS-LD-AT)₂ platform, thus creating two separate reaction chambers, reminiscent of the porcine fatty acid synthase architecture (4, 5). However, Lsd14's two reaction chambers are substantially different from each other because of how the KR domains are positioned. In chamber I, the KS', AT, and KR' active site entrances all face the center of the reaction chamber, where ACP is located. However, in chamber II, only the KS and AT' active site entrances face the center of the reaction chamber. Furthermore, ACP is docked to the AT chamber I, whereas no ACP is present in chamber II. In this configuration, transacylation, condensation, and β-keto group reduction can only take place in chamber I. Three structural features support this hypothesis. First, the Lsd14 sequence contains an ADE that places the second ACP also in chamber I, close to the observed ACP. Second, the C termini of both KR domains are located in chamber I, and because KR and ACP are tethered by a 12-residue linker, both ACPs likely reside in chamber I. Third, entrance to the KR active site is pointed away from chamber II, and therefore reduction cannot take place in this reaction chamber. Although chain elongation and β -keto group modification are expected to take place only in chamber I, chamber II can attain the same domain configuration as chamber I through an ~260° rotation of (KR)2. Overall, the asymmetric domain organization in Lsd14 indicates that its two reaction chambers operate asynchronously, and only one chamber performs polyketide chain synthesis at any given time.

Interactions at the AT-ACP interface

In reaction chamber I, ACP is docked to the AT. Because apo-Lsd14 crystals were used for this study, ACP lacks the P-pant group modification. ACP residue S1526, which would bear the ~20-Å-long P-pant group in holo-Lsd14, is pointed at the catalytic residue S657 of AT (S1526 to S657 distance = 22.5 Å) (Fig. 2A).Multiple hydrogen bond and salt bridge interactions are present at the ACP docking site (Fig. 2B). We tested the requirement of these interactions by performing a multiple turnover assay using recombinantly expressed (DD-KS-LD-AT)2 and ACP fragments of Lsd14 (fig. S4, A and B) (16). Among residues interacting at the AT-ACP interface, ACP residues are highly conserved across modular PKSs, whereas AT residue E845 varies according to the

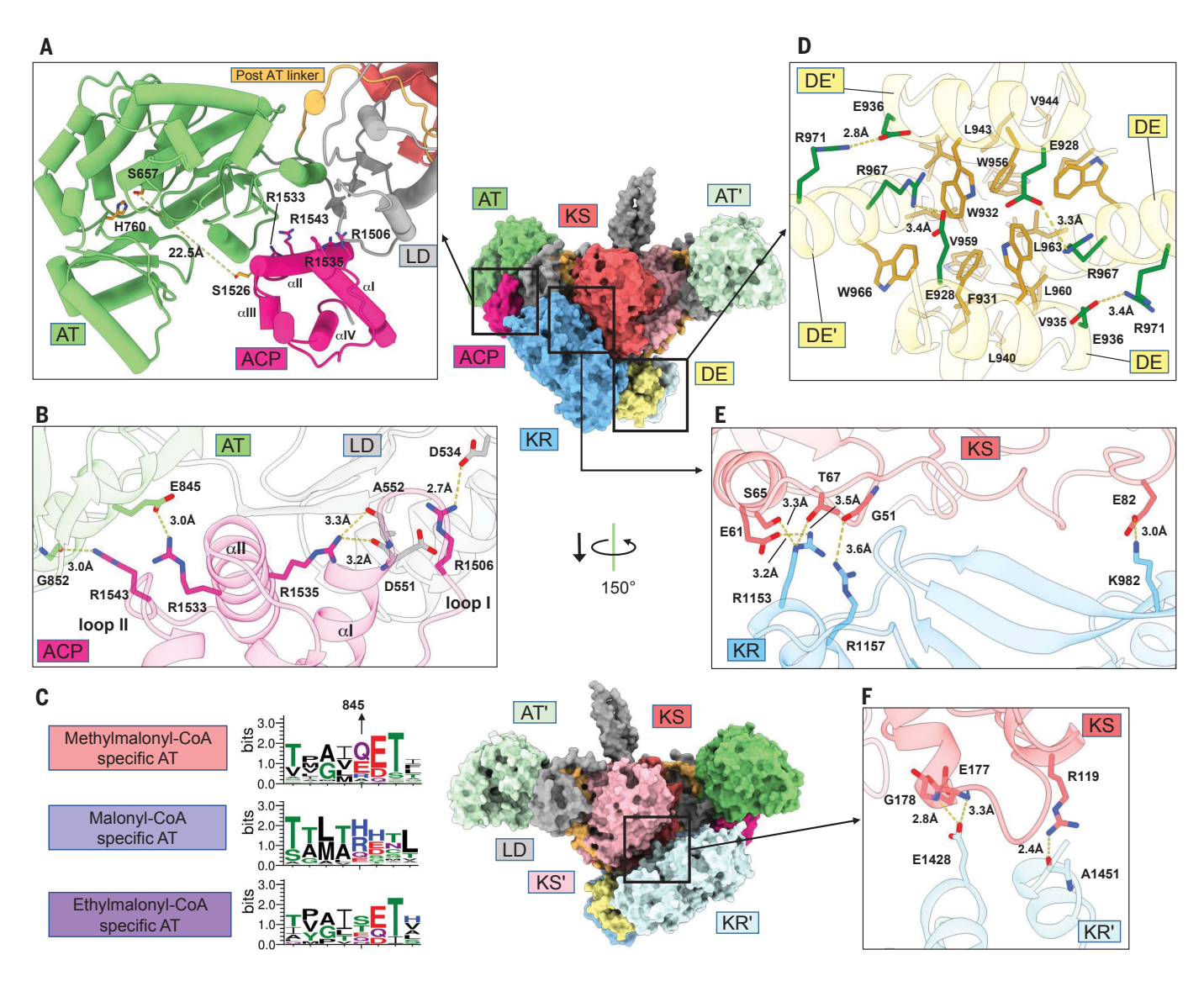


Fig. 2. Interdomain interactions of apo-Lsd14 trapped in the transacylation step. (A) ACP docking site. (B) Interactions at the AT-ACP interface. (C) WebLogo image showing relative frequency of amino acids at position 845 in AT sequences. (D) Interactions at the DE. (E and F) Interactions at the KR-KS and KR'-KS interfaces.

identity of the partner acyl-CoA (Fig. 2C and fig. S5). Typically, ATs specific for methylmalonyl-CoA and ethylmalonyl-CoA have an acidic or a polar residue at position 845, whereas ATs specific for malonyl-CoA have a basic residue. This structural variation may allow the ACP to dock to the AT in a slightly different orientation depending on the identity of the extender unit found on the AT. Our Lsd14 crystal structure contains a second AT-ACP interface, but this interaction appears to involve the AT' from a crystallographic symmetry mate and seems to be artificial (fig. S4B and fig. S6, A and B).

The tertiary structure of AT and AT in Lsd14 are nearly identical (RMSD = 0.3 Å). Furthermore, the structure of ACP in the Lsd14 crystal structure is highly similar to the solution nuclear magnetic resonance structure of stand-

alone ACP2 from DEBS (PDB 2JU2, RMSD = 1.5 Å) (fig. S6C) (17). In addition to the *cis*-AT-ACP complex in the current work, crystal structures of two *trans*-AT-ACP complexes, DSZS AT-ACP1 (PDB 5ZK4) (18) and VinK-VinL (PDB 5CZD) (19), have been reported. Unexpectedly, the AT-ACP interaction is not conserved in these three structures (fig. S7), suggesting that ACP has latitude in how it docks to the AT.

Architecture and specific interactions of the DE-KR domains

We confirmed the KR activity of Lsd14 using a colorimetric KR activity assay (fig. S8). The KR domains dimerize through the DE, forming a single (DE-KR)₂ unit in which KR and KR' lie parallel to each other in a head-to-head manner, but their active site entrances face oppo-

site directions (Fig. 1C). The two DE domains form a six-helix bundle that is held together by multiple hydrophobic and hydrogen bond interactions (Fig. 2D and figs. S9A and S10). DE/ DE' helices I and III make specific interactions with KR/KR' in the crystal structure (fig. S9, B and C, and fig. S10). (DE-KR)2 is docked to the KS/KS' dimer in such a way that it occupies chamber I more than chamber II (Fig. 1). Furthermore, the active site entrance of KR' points toward KS' in reaction chamber I, whereas the active site entrance of KR faces away from either reaction chamber (fig. S11). (DE-KR)₂ is a prominent, symmetry-breaking element in the Lsd14 architecture and has important functional implications that are described further below. (DE-KR)₂ appears to be mobile, as indicated by the relatively high B-factors calculated for KR/KR' and DE/DE' residues

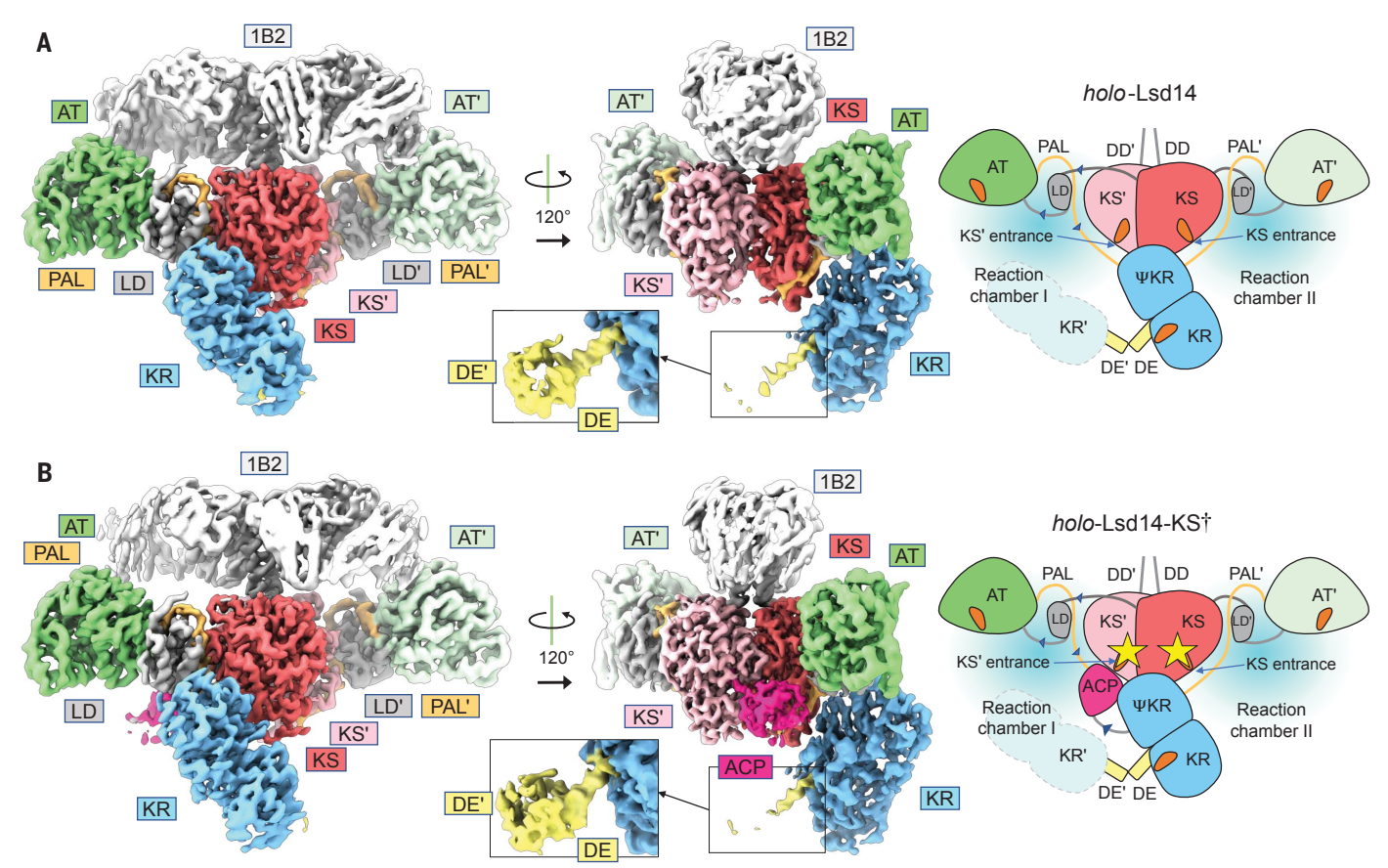


Fig. 3. Cryo-EM maps of *holo*-Lsd14 with the DEBS docking domain bound to the 1B2 Fab fragment with and without treatment with KS substrate analog. Composite maps made by combining unsharpened focused maps are shown.

(A and B) *holo*-Lsd14-DD*+1B2 (A) and *holo*-Lsd14-DD*-KS†+1B2 [*holo*-Lsd14-DD*+1B2

treated with KS substrate analog; probable acylation is denoted by a yellow star on

the KS active sites (B)]. The map threshold value is 14 and 12 for (A) and (B), respectively. Magnified version shows map for DE/DE' interface at lower map threshold values of 7.7 and 5.5 for (A) and (B), respectively. A cartoon representation depicting the Lsd14 domain organization and location of active sites (orange) is shown on the right. Fab has been omitted from the cartoon for clarity.

compared with the rest of the protein (fig. S12). The overall organization of (DE-KR)₂ in Lsd14 is similar to the crystal structure of the isolated (DE-KR)₂ from the amphotericin PKS (PDB 4L4X) and the spinosyn PKS (PDB 4IMP) (20, 21). However, the relative positioning of the KR domains in spinosyn PKS differs from the other two structures because of flexing of helix III of the DE (fig. S9, D and E).

In reaction chamber I, both KR and KR' contact the KS and establish multiple hydrogen bond and salt bridge interactions (Fig. 2, E and F). KS residues E61/S65/T67, and E82 form two regions with negative electrostatic surface potential that interact with positively charged surfaces formed by KR residues R1157/R1153 and K982, respectively (fig. S13).

Cryo-EM structure of holo-Lsd14-Fab

To investigate Lsd14's domain organization in other states of the PKS reaction cycle, we conducted cryo-EM analysis of *holo-*Lsd14. Our initial attempts resulted in extensive dissocia-

tion of the Lsd14 homodimer into monomeric species on cryo-EM grids (fig. S14A). Our efforts to preserve the Lsd14 dimer integrity through buffer exchange, ligand addition, and chemical cross-linking failed to produce a stable Lsd14 homodimer suitable for cryo-EM study. We predicted that Fab 1B2, which was previously used by the Khosla group for structural study of the DEBS PKS (22), and also in the accompanying article (23), would bind and stabilize the Lsd14 homodimer because the residues involved in Fab binding are conserved in Lsd14 and DEBS. However, Fab 1B2 failed to bind to Lsd14, which prompted us to prepare an Lsd14 variant, Lsd14-DD*, which contains the DD of DEBS module 3, 1B2 readily bound to Lsd14-DD*, and the resulting complex, Lsd14-DD*+1B2, was suitable for cryo-EM analysis (fig. S14B). We also found that addition of methylmalonyl-CoA, the native AT substrate, was essential for visualizing an ordered KR domain. These strategies produced a 3.1-Å-resolution cryo-EM map of holo-Lsd14-DD*+1B2 (Fig. 3A). The final structure contains two 1B2 molecules,

with each Fab making contact with DD, KS, and AT, similar to the crystal structure of DEBS module 3 (DD-KS-LD-AT)₂ bound to 1B2 Fab (22) (fig. S15). The Lsd14 (KS-LD-AT)₂ in the cryo-EM structure has the same overall extended conformation as that in the Lsd14 crystal structure. Our in vitro enzyme assay showed that 1B2 did not affect the rate of transacylation (fig. S4D). Unlike in the Lsd14 crystal structure, only one KR is observed, and no ACP is visible in the cryo-EM structure. The local resolution of the DE/DE' interface in the cryo-EM maps is low, likely because of the flexibility of the DE. However, visualization of the crvo-EM maps at a lower threshold reveals that the DE dimerizes in the cryo-EM maps, indicating that the (DE-KR)₂ is intact in the cryo-EM sample, although KR' domain is unresolved (fig. S16). The interface between KR and KS is identical in the Lsd14 crystal and cryo-EM structures (fig. S17). We also imaged the apo form of Lsd14-DD*+1B2 under the same condition and found that the maps were essentially indistinguishable (fig. S18).

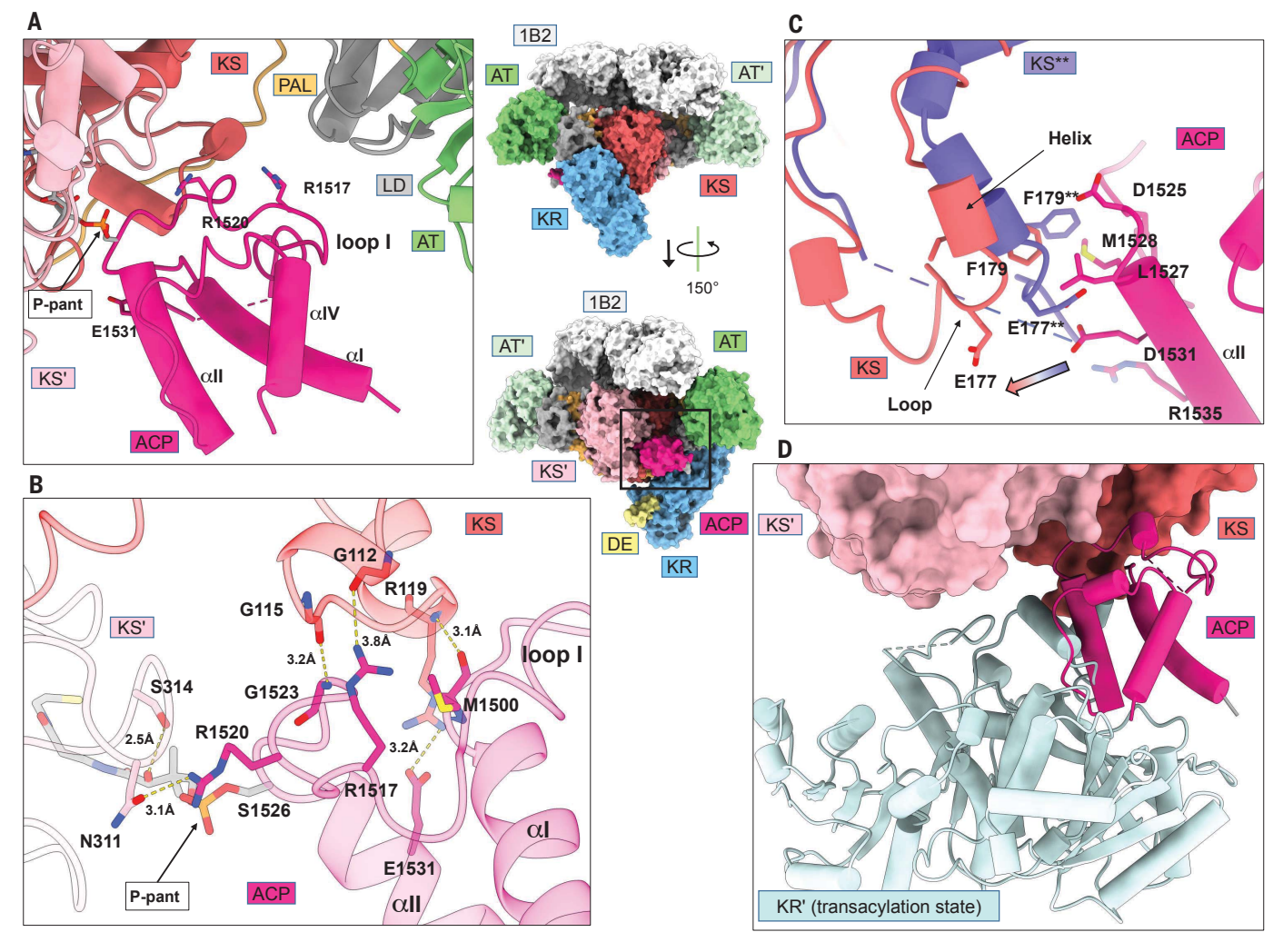


Fig. 4. Interdomain interactions of *holo*-Lsd14 trapped in the condensation step. (A) ACP docks in a cleft formed between the KS dimer and the LD-AT and the P-pant group stretches into the KS' active site. (B) Interactions at the ACP-KS-KS' interface. (C) Rearrangement of the KS helix + loop upon ACP binding. KS domain from the *holo*-Lsd14-DD*+1B2 (purple) superimposed

on the KS domain from the *holo*-Lsd14-DD*-KS \uparrow +1B2 structure (salmon). Direction of the movement of KS helix + loop motif upon ACP binding is indicated by the multicolored arrow. (**D**) Region where ACP binds to KS during the condensation step partially overlaps with the region where KR' binds to KS during the transacylation step.

Cryo-EM structure of holo-Lsd14-Fab stalled at the condensation step

Next, we treated holo-Lsd14-DD*+1B2 with the KS substrate analog 2-acetaminoethyl-thio-3-oxobutanoate and subjected this sample to cryo-EM analysis (fig. S14D). We obtained a cryo-EM map for this sample, referred to as holo-Lsd14-DD*-KS†+1B2, at an overall resolution of 3.1 Å (Fig. 3B). In this second cryo-EM structure, ACP is docked to KS in reaction chamber I. This interaction is required for the condensation step of the PKS cycle. The organization of KS/KS', AT/AT', and KR in holo-Lsd14-DD*-KS†+1B2 is the same as that of holo-Lsd14-DD*+1B2. We determined that the ACP in this structure is connected to KR, not KR', based on the partially visible map density for the KR-ACP linker and linker length constraints (fig. S19).

The active site of KS' in reaction chamber I and that of KS in chamber II can be accessed through their dedicated side entrances. In the holo-Lsd14-DD*-KS†+1B2 structure, ACP is docked at the KS' side entrance in a cleft between the KS-KS' dimer and the LD-AT domain, with its P-pant group stretched toward the KS' active site (Fig. 4A). Residues in loop I and helix II of the ACP make specific interactions with a loop region in KS (G112-R119) and KS' (N311) (Fig. 4B). The ACP and KS residues involved in these interactions are highly conserved in modular PKSs (fig. S20). The Lsd14 KS-ACP interface is consistent with previously reported biochemical results for DEBS (24), confirming the importance of ACP loop I and helix II for the ACP-KS interaction.

There is clear map density for the P-pant group attached to S1526 of ACP (fig. S21A).

KS residue S314 forms a hydrogen bond with the carbonyl oxygen atom of the P-pant group (Fig. 4B). This serine was previously predicted to stabilize the binding of methylmalonyl-ACP to KS in DEBS (25). We also observed extra map density extending from the terminal sulfur atom of both the P-pant group and the catalytic cysteine (C210) of the KS domain (fig. S21A). The extra map density on the P-pant arm is likely the methylmalonyl moiety, the product of AT-catalyzed transacylation reaction. The extra map density at C210 may be caused by acylation because it was not observed in the holo-Lsd14-DD*+1B2 map, although the map density in this region is insufficient to accurately model this feature (fig. S21B).

Comparison of the region of KS that interacts with the ACP in *holo*-Lsd14-DD*-KS†+1B2

with the equivalent region in holo-Lsd14-DD*+1B2 revealed that the helix + loop motif within the KS (175-184) undergoes reorganization upon binding to ACP (Fig. 4C). The ACP-KS docking mode in the holo-Lsd14-DD*-KS†+ 1B2 structure is similar to that observed in the 7.1-Å-resolution cryo-EM structure of the CTB1iterative PKS fragment (26) (fig. S22). R119 of KS, which forms a salt bridge with E1531 of ACP at the Lsd14 ACP-KS interface, was shown to be important for nor-toralactone production by CTB1 PKS (R461 in CTB1) (26). The cis-ACP-KS interfaces of Lsd14 and CTB1 are distinct from the previously observed trans-ACP-KS interfaces: cis-ACPs dock to the KS dimer by orienting loop I toward the KS, whereas trans-ACPs orient loop I away from the KS dimer (fig. S22).

In the Lsd14 crystal structure, ACP is docked to the AT (Fig. 2A), whereas KR' is docked to the KS (Fig. 2F). In the holo-Lsd14-DD*-KS†+ 1B2 cryo-EM structure, ACP is docked to the KS/KS' dimer at the KS' active site entrance. Overlaying these two structures shows that the location of ACP in the cryo-EM structure overlaps with location of KR' in the crystal structure (Fig. 4D). This indicates that the ACP cannot directly translocate from AT to KS' upon completion of the transacylation reaction because the ACP docking site on KS' is sterically blocked by KR'. Therefore, KR' must first undock from the KS, which would enable the ACP to dock to the KS' and allow condensation reaction to ensue. This process would ensure that ACP gains access to KS' only after transacylation has taken place.

Discussion

Both the crystal and cryo-EM structures of Lsd14 show an intriguing asymmetrical architecture that contrasts with previous PKS models derived from chemical cross-linking, domain complementation, cryo-EM, and small-angle x-ray scattering experiments, which depicted a perfect, or near-perfect, twofold symmetry (22, 27-29). In our Lsd14 structures, ACP is found only in one of the two reaction chambers docked either to the AT or to the KS. The second ACP is not visible in the experimental maps, which suggests that it is not docked to any domain. Additionally, the presence of the ADE in the Lsd14 sequence suggests that the two ACPs remain close together. On the basis of these observations, we propose a pendulum clock model for Lsd14. In this model, (DD-KS-LD-AT)₂ is static while (DE-KR-ACP)₂ traverses between the two reaction chambers through a swinging motion with the DE as the fulcrum such that the two reaction chambers are used nonconcurrently (fig. S23). We hypothesize that chamber I performs extender unit transacylation, polyketide chain elongation, and β-keto group reduction, whereas chamber II becomes transacylated with the growing polyketide chain from the upstream PKS. Next, the (DE- ${\rm KR\text{-}ACP})_2$ pendulum swings to the opposite side and performs the same set of reactions that was just completed in chamber I. Alternatively, the two reaction chambers may be used stochastically, but only one polyketide product would be formed at a time.

PKS engineering has the potential to generate countless new polyketides for drug discovery. It has already been demonstrated that domain substitution, insertion, and deletion in modular PKSs leads to the production of new natural product analogs (30). However, the overall yield is drastically decreased, and mixed products are often formed. These deficiencies are most likely caused by protein misfolding and suboptimal domain-domain interactions resulting from introduction of non-native domains. Our Lsd14 structures show that the constituent domains in a modular PKS are elaborately organized and interact with one another through numerous specific interactions. To obtain the best result, domain manipulations in PKSs must be executed in a manner that preserves the native protein fold and interaction surfaces. Our work provides a high-resolution blueprint for designing minimally invasive domain manipulations. However, the current work only provides insight into the structure and function of a single-module PKS consisting of KS, AT, KR, and ACP domains. If we are to realize routine rational PKS engineering, future work is needed to reveal the workings of PKSs that also contain DH, ER, and TE domains and those with multiple modules on the same polypeptide chain. Furthermore, we must elucidate the structural basis of intermodule and inter-PKS communication.

Our study illustrates how x-ray crystallography and cryo-EM may be used concurrently to extract the maximum amount of protein structural information. However, we could not use native Lsd14 for cryo-EM analysis because the PKS dimers disintegrated into monomers when placed on the cryo-EM grid. We solved this problem by substituting the N-terminal docking domain in Lsd14 with the counterpart from a DEBS PKS and then applying the Fab fragment that binds to the DEBS docking domain. By comparison, our crystal structure is that of the native full-length Lsd14 and thus accurately reflects the PKS as it is found in nature. Comparison of the crystal and cryo-EM Lsd14 structures shows that Fab binding only causes a slight movement of the docking domain, indicating that the cryo-EM Lsd14 structure is biologically relevant. The application of Fab to stabilizing the PKS homodimer may facilitate future structural studies of other modular PKSs using cryo-EM.

REFERENCES AND NOTES

 D. E. Cane, W. D. Celmer, J. W. Westley, J. Am. Chem. Soc. 105, 3594–3600 (1983).

- J. Cortes, S. F. Haydock, G. A. Roberts, D. J. Bevitt, P. F. Leadlay, *Nature* 348, 176–178 (1990).
- S. Donadio, M. J. Staver, J. B. McAlpine, S. J. Swanson, L. Katz, Science 252, 675–679 (1991).
- 4. T. Maier, S. Jenni, N. Ban, Science 311, 1258-1262 (2006).
- T. Maier, M. Leibundgut, N. Ban, Science 321, 1315–1322 (2008).
- E. J. Brignole, S. Smith, F. J. Asturias, Nat. Struct. Mol. Biol. 16, 190–197 (2009).
- F. M. C. Benning et al., ACS Nano 11, 10852–10859 (2017).
- A. Migita et al., Biosci. Biotechnol. Biochem. 73, 169–176 (2009).
- A. Minami et al., J. Am. Chem. Soc. 134, 7246–7249 (2012).
- Y. Shichijo et al., J. Am. Chem. Soc. 130, 12230–12231 (2008).
- 11. K. Hotta et al., Nature 483, 355-358 (2012).
- 12. F. T. Wong et al., J. Am. Chem. Soc. 137, 86-89 (2015).
- Y. Tang, A. Y. Chen, C.-Y. Kim, D. E. Cane, C. Khosla, Chem. Biol. 14, 931–943 (2007).
- Y. Tang, C.-Y. Kim, I. I. Mathews, D. E. Cane, C. Khosla, *Proc. Natl. Acad. Sci. U.S.A.* 103, 11124–11129 (2006).
- 15. J. R. Whicher et al., Chem. Biol. 20, 1340-1351 (2013).
- 16. B. J. Dunn, D. E. Cane, C. Khosla, *Biochemistry* **52**, 1839–1841
- V. Y. Alekseyev, C. W. Liu, D. E. Cane, J. D. Puglisi, C. Khosla, Protein Sci. 16, 2093–2107 (2007).
- A. Miyanaga et al., J. Am. Chem. Soc. 140, 7970–7978 (2018).
- A. Miyanaga, S. Iwasawa, Y. Shinohara, F. Kudo, T. Eguchi, Proc. Natl. Acad. Sci. U.S.A. 113, 1802–1807 (2016).
- J. Zheng, S. K. Piasecki, A. T. Keatinge-Clay, ACS Chem. Biol. 8, 1964–1971 (2013).
- 21. J. Zheng, C. D. Fage, B. Demeler, D. W. Hoffman,

 A. T. Koatingo-Clay, ACS Cham, Biol. 8, 1263–1270 (2013)
- A. T. Keatinge-Clay, ACS Chem. Biol. 8, 1263–1270 (2013).
- 22. X. Li et al., J. Am. Chem. Soc. 140, 6518–6521 (2018).
- D. P. Cogan et al., Science 374, 729–734 (2021).
 S. Kapur, A. Y. Chen, D. E. Cane, C. Khosla, Proc. Natl. Acad.
- S. Kapur, A. Y. Chen, D. E. Cane, C. Khosla, *Proc. Natl. Aca Sci. U.S.A.* 107, 22066–22071 (2010).
- T. Robbins, J. Kapilivsky, D. E. Cane, C. Khosla, *Biochemistry* 55, 4476–4484 (2016).
- 26. D. A. Herbst et al., Nat. Chem. Biol. 14, 474-479 (2018).
- 27. J. Staunton et al., Nat. Struct. Biol. 3, 188-192 (1996).
- C. M. Kao, R. Pieper, D. E. Cane, C. Khosla, *Biochemistry* 35, 12363–12368 (1996).
- 29. S. Dutta et al., Nature 510, 512-517 (2014).
- 30. M. Klaus, M. Grininger, *Nat. Prod. Rep.* **35**, 1070–1081 (2018).

ACKNOWLEDGMENTS

We thank C. Khosla for providing the 1B2 Fab expression plasmid. x-ray diffraction data were collected at the Stanford Synchrotron Radiation Lightsource (SSRL), Advanced Light Source (ALS), and Advanced Photon Source (APS), Use of the SSRL, SLAC National Accelerator Laboratory, is supported by the U.S. Department of Energy (DOE), Office of Science, Office of Basic Energy Sciences under contract no. DE-AC02-76SF00515. The SSRL Structural Molecular Biology Program is supported by the DOE Office of Biological and Environmental Research and by the National Institutes of Health, National Institute of General Medical Sciences (including P41GM103393). ALS is a U.S. DOF Office of Science User Facility under contract no. DE-AC02-05CH11231. APS is a DOE Office of Science User Facility operated for the DOE Office of Science by Argonne National Laboratory under contract no. DE-ACO2-06CH11357. We acknowledge the Cornell Center for Materials Research (CCMR), notably K. Spoth and M. Silvestry-Ramos, for access and support of electron microscopy sample preparation and data collection (NSF MRSEC program, DMR-1719875). We also thank the staff of the Proteomics and Metabolomics Facility at Cornell Institute of Biotechnology for conducting HPLC-MS. The contents of this publication are solely the responsibility of the authors and do not necessarily represent the official views of NIGMS, NIH, or DOF. Funding: This work was supported by National Institutes of Health grants R01GM138990 to C.-Y.K., R35GM136258 to J.C.F., and 5U54MD007592. Author contributions: C.-Y.K. conceived and supervised the project, S.R.B. expressed, purified, and crystallized Lsd14. S.R.B. and I.I.M. conducted x-ray diffraction experiments. S.R.B., I.I.M., and C.-Y.K. solved the Lsd14 crystal structure, S.R.B. performed cryo-EM data acquisition and analysis. J.C.F. supervised the cryo-EM experiments. S.R.B. and C.-Y.K. wrote the manuscript with

input from all authors. **Competing interests:** The authors declare no competing financial interests. **Data and materials availability:** All atomic coordinates and structure factors have been deposited in the Protein Data Bank (accession codes: 756B, 756C, and 756D). All cryo-EM maps have been deposited in the Electron Microscopy Data Bank (accession codes: EMD-24862, EMD-24863, EMD-24864, EMD-24865, EMD-24866, EMD-24871, EMD-24877, EMD-24873, EMD-24871, EMD-24873, EMD-24874, EMD-24875,

and EMD-24880). All other data are presented in the main text or the supplementary materials.

SUPPLEMENTARY MATERIALS

science.org/doi/10.1126/science.abi8532 Materials and Methods Supplementary Text Figs. S1 to S28 Tables S1 to S5 References (31–56) MDAR Reproducibility Checklist

View/request a protocol for this paper from Bio-protocol.

5 April 2021; accepted 21 September 2021 10.1126/science.abi8532

7 of 7



Modular polyketide synthase contains two reaction chambers that operate asynchronously

Saket R. Bagdelrimpan I. MathewsJ. Christopher FrommeChu-Young Kim

Science, 374 (6568), • DOI: 10.1126/science.abi8532

Big molecules build small

Actinomycete bacteria are prolific producers of bioactive small molecules such as polyketide antibiotics. These molecules are built by the addition of short carbon units to a growing, protein-tethered chain, either iteratively as in fatty acid synthesis or in a modular fashion by a hand-off from one distinct enzyme complex to the next. Bagde *et al.* and Cogan *et al.* report structures of polyketide synthase modules in action, taking advantage of antibody stabilization of one of the domains. Both groups visualized multiple conformational states and an asymmetric arrangement of domains, providing insight into how these molecular assembly machines transfer substrates from one active site to another. —MAF

View the article online

https://www.science.org/doi/10.1126/science.abi8532

Permissions

https://www.science.org/help/reprints-and-permissions

Use of think article is subject to the Terms of service